# Chapter 7
# On the Occurrence of Elastic Singularities in Compressed Thin Sheets: Stress Focusing and Defocusing

**Alain Pocheau**

**Abstract** Compressing thin sheets usually yields the formation of singularities which focus curvature and stretch on points or lines. In particular, following the common experience of crumpled paper where a paper sheet is crushed in a paper ball, one might guess that elastic singularities should be the rule beyond some compression level. In contrast, we show here that, somewhat surprisingly, compressing a sheet between cylinders makes singularities spontaneously disappear at large compression. This "stress-defocusing" phenomenon is qualitatively explained from scale invariance and further linked to a criterion based on a balance between stretch and curvature energies on defocused states. This criterion is made quantitative using the scalings relevant to sheet elasticity and compared to experiment. These results are synthesized in a phase diagram completed with plastic transitions. They end up with a renewed vision of elastic singularities as a thermodynamic condensed phase where stress is focused, in competition with a regular diluted phase where stress is defocused. Different compression routes may be followed in this diagram by managing differently the two principal curvatures of a sheet, as experimentally achieved here. In practice, besides the famous Elastica and crumpled paper routes, this offers interesting alternatives for compressing a sheet with an amazing spontaneous regularization of geometry and stress that repels the occurrence of plastic damages.

A. Pocheau (✉)
IRPHE, Aix-Marseille Université, 49, rue F. Joliot Curie, B.P. 146,
13384 Marseille Cedex 13, France
e-mail: alain.pocheau@irphe.univ-mrs.fr

## 7.1 Introduction

Thin envelops, thin layers, or thin films stand as an efficient mean to separate domains, treat surfaces, or confine volumes. Examples include graphene sheets [1], epitaxial deposit at sub-micrometric scales [2], membranes at micrometric scales [3], packaging at sub-millimeter scales [4], metallurgical structures at millimeters scales and beyond, and geological layers at even larger scales [5], the scale meaning here the thickness of the object. Their common feature is to display a weak dimension, their thickness, in comparison to their length and width, according to which most of their properties can be recovered by treating them as 2D surfaces involving flexural effects. In many instances, however, these thin sheets undergo geometrical constraints that force them to fit into a reduced space. They then have to adapt their form to restrictive conditions, something they may do smoothly or sharply, i.e., with small or large curvature as compared to their inverse thickness. In the latter case, they then escape the 2D surface assumption, especially at the locations of large curvature where they show up surface singularities. The occurrence of these singularities is essential in various instances. In practice, they involve large elastic stresses and 3D interactions that make them escape the 2D modeling and possibly even the physical regime of the remainder of the sheet. In particular, the sheet properties are usually altered there regarding electronic properties, robustness, or even the elasticity regime, with a possible transition to plasticity at the core of singularities.

On a more general viewpoint, these singularities enable the elastic stress to relax in the remaining sheet parts: the bending stress for the so-called ridges [6–8] and the stretching stress for the so-called developable cones (d-cones) [9–12]. In this sense, they appear as inner degrees of freedom for adapting the geometric constraints imposed to compressed sheets. Doing so, they thus focus the sheet's stress on the singularity cores, a phenomenon called stress focusing [13].

Stress focusing is a particular example of the phenomenon of energy focusing which widely occurs in out-of-equilibrium systems beyond some distance to equilibrium. Some of its manifestations are vorticity concentration in turbulent fluids, rogue waves occurrence, shock wave formation in thermodynamic systems, dielectric breakdown in media submitted to electrostatic field, fracture in stressed solids, etc. (Fig. 7.1). In all these phenomena, the energy density which moved the system far from equilibrium spontaneously turned from a homogeneous distribution to a highly localized concentration. This phenomenon thus stands as an emblematic example of self-organization.

Stress focusing is all the more surprising that one might have naively guessed that energy seeks to spread over instead of concentrating on singular objects. In particular, this energy focusing goes against the equidistribution of energy and thus questions the statistical description of these systems. Moreover, the emergence of definite locations or structures (sometimes called "coherent structures") where energy is concentrated, largely governs the system behavior and its properties. This
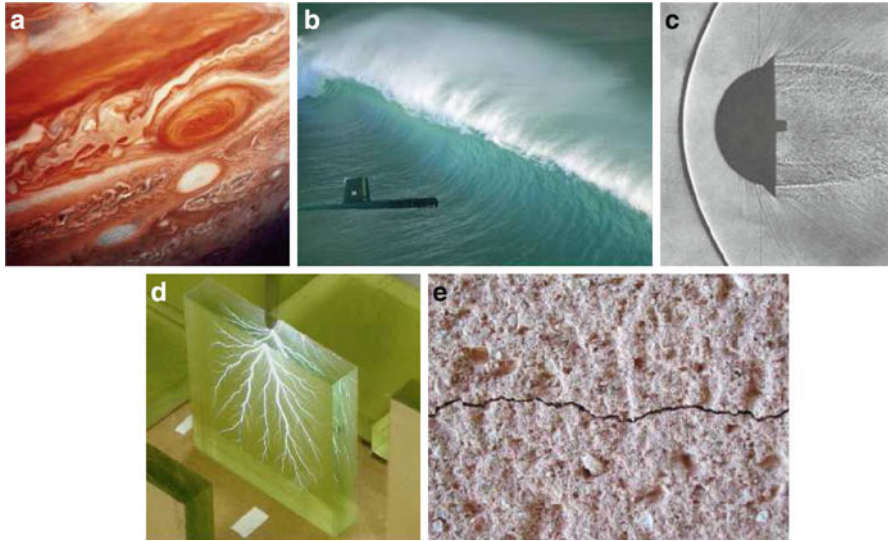
**Fig. 7.1** Examples of energy focusing : (**a**) vorticity concentration in the Jupiter red spot taken by Voyager 2 (Credit NASA image), (**b**) rogue wave (Credit Toptenz.net) (**c**) shock wave produced by blunt bodies (Credit NASA image) (**d**) dielectric breakdown yielding so-called lichtenberg figures (Credit Theodore Gray as shown on http://www.capturedlightning.com) (**e**) fracture in solid concrete

is why vast efforts have been devoted in all the above systems to characterize the conditions for energy focusing as well as the resulting energetically dense structures and their implications.

Here, we address this issue in the context of sheet compaction where forms and stresses are governed by elasticity. Two major rules for self-organization are then in order. First, as there is no intrinsic scale in elasticity, scale invariance and scaling arguments apply. Second, as elasticity is non-dissipative in its elastic regime, energy landscapes can be used to infer the preferred states, including those involving elastic singularities. In particular, the occurrence of a stress-focused state may be understood as the fact that it became energetically preferred as compared to a stress-distributed state. Applying both these rules should then largely help elucidating stress focusing, but with possible surprises. In particular, the popular example of crumpled paper where the compaction of a sheet in a ball generates scars (Fig. 7.3-right) usually yields the common guess that singularities and stress focusing should irremediably persist when increasing compaction. On the opposite, we shall find here that, surprisingly, the two above rules deny this belief, in the sense that scalings imply that singular states should no longer be preferred at large compaction, if they previously were: stress should thus *defocus* at large compaction.

This phenomenon of stress defocusing implies that the ultimate state of a compressed sheet should be smooth and regular. Its actual existence will be evidenced on a dedicated experiment and the apparent paradox regarding the usual

experience of crumpled paper will be clarified [14]. This will enable us to identify singularities as a thermodynamic condensed phase surrounded in phase space by the regular diluted phase corresponding to regular geometries and defocused stress. In particular, the persistence of singularities on some actual compression routes will be shown to refer to plasticity instead of elasticity. In this regard, the popular demonstration of paper crumpling by the hands will appear as a misleading example of (linear) elasticity since the singularities that form should disappear at large compression but actually do not because of plasticity only.

Altogether, this study will thus provide a modified vision of the nature of elastic singularities and of sheet adaptation to compression. In particular, on compression routes, singularities, instead of being the rule beyond some compression level, will actually appear as a transient state.

In the following, we first emphasize in Sect. 7.2 the relevance of an intermediate compression route between Elastica and crumpled paper to address singularity occurrence. We then recall in Sect. 7.3 some basics on linear elasticity, especially regarding the Gaussian curvature and its implications. We then report in Sect. 7.4 an experiment of compression between cylinders and the resulting evidence of stress defocusing. Energy arguments for stress focusing or defocusing are then addressed in Sect. 7.5 together with scaling arguments. They are applied in Sect. 7.6 to show the necessity of defocusing and derive a phase diagram for singularities, taking into account plasticity. This is followed by a conclusion on the implications of this study for the nature of singularities in elasticity.

## 7.2 On Singularity Occurrence in Sheet Elasticity: From Elastica to Crumpled Paper

On thin sheets, two kinds of stresses may be defined: one related to the stretch of a sheet viewed as a 2D surface and one related to the sheet's curvature [11, 13, 15]. As regards to stress focusing, it appears that the stretch stress is the dominant stress on singularities and on the non-singular states on which they appear. Accordingly, singularity formation actually corresponds to focusing that stretch on singularities, leaving in between unstretched but possibly curved domains.

Interestingly, stretch is generated by sheet deformations that involve a Gaussian curvature $G$, actually equal to the product of the principal curvatures $c_1$, $c_2$, at a point: $G = c_1 c_2$ (see Sect. 7.3.2). Usually, compacting sheets cannot avoid generating Gaussian curvatures, thus stretch, until provoking stress focusing in singularities, as on crumpled paper (Fig. 7.3-right). To improve our understanding of this phenomenon, the clue of this work is to notice that, as *two* principal curvatures are involved in the Gaussian curvature $G$, several physically different compacting routes may be explored depending on the correlations involved between them. In particular, three different routes worth being distinguished:

- Elastica: $G = 0$, $c_2 = 0$
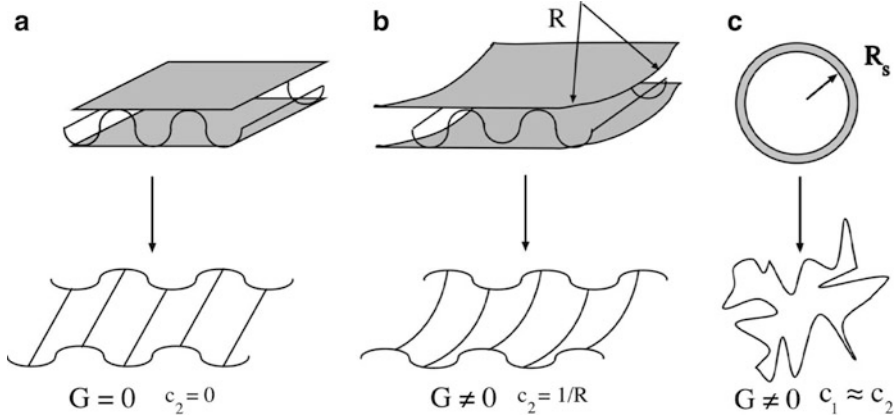
**Fig. 7.2** Different compression routes regarding singularity occurrence: (**a**) Compression between flat plates. Fold axes are straight so that a principal curvature $c_2$ is forced to vanish: $c_2 = 0$, $G = 0$. The compression route shows no singularity. (**b**) Compression between cylinders. Fold axes are bent by the cylinders so that a principal curvature $c_2$ is forced to be that of the cylinders: $c_2 = 1/R$, $G \neq 0$. (**c**) Compression by a shrinking sphere of radius $R_s$. This corresponds to the crumpled paper configuration. Principal curvatures do not vanish and are about the same: $c_1 \equiv c_2 \equiv 1/R_s$, $G \neq 0$. This generates singularities

One may annihilate one curvature, simply by forbidding curvature on a direction (Fig. 7.2a). This is achieved in practice by compressing sheets in between parallel plates. Then, a family of parallel folds is generated by iterated bucklings, all parallel to one direction of the plates along which they are thus uncurved (Fig. 7.3a). One curvature, $c_1$, is thus provided by folds but the other, $c_2 = 0$, vanishes since it corresponds to the uncurved fold axis direction. Then $G = 0$ so that no stretch is generated and, therefore, no singularity at any compression level. The sheet is thus equivalent to a set of rods whose elastic evolutions are modeled by the so-called Euler's "Elastica" [16, 17].

- Isotropic compression and crumpled paper: $G \neq 0$, $c_1 \equiv c_2$.
  On the opposite, one may force the two principal curvatures not to vanish and to take statistically similar values (Fig. 7.2c). This is achieved in practice by compressing a sheet into a shrinking spherical domain, as when crumpling a paper with hands (Fig. 7.3-right). Then, because of isotropy, the two principal curvatures are both nonzero and statistically equivalent $c_1 \equiv c_2$, so the term "isotropic" compression. A Gaussian curvature is thus generated and increases with compaction until singularities occur.

- Anisotropic compression: $G \neq 0$, $c_2$ fixed
  Finally, a third route, actually intermediate between the two above opposite routes, may be designed by compressing sheets not between plates or a sphere but between cylinders (Fig. 7.2b). Taking the cylinders curvature radius $R$ large compared to the gap between them, this looks locally similar to a compression in between parallel plates so that a family of parallel folds is expected. However,

**Fig. 7.3** *Left*: buckling cascade on a sheet compressed between parallel plates [18]. *Right*: crumpled paper crushed in hands

the fixed cylinder curvature nevertheless bends their fold axes and this makes all the difference. The curvature $c_2$, instead of being zero as on the Elastica route, is fixed here to a nonzero value equal to the inverse cylinder curvature radius $c_2 = 1/R$. A nonzero Gaussian curvature is then generated yielding singularity formation beyond a compression level. However, in contrast with crumpled paper, the imposed curvature $\bar{c}_2$ of the fold axes is kept constant here. It is thus decorrelated from the remaining fold curvature $c_1$, so the term "anisotropic" compression. Should this difference be relevant and yield a different sheet evolution?

The experiment reported in Sect. 7.4 will provide the answer. Interestingly, we note that the end result could be anticipated from scale invariance, but we postpone the explanation to Sect. 7.6.1.

## 7.3   Basics on Linear Elasticity of Sheets

The linear response of materials to deformation has been synthesized by Robert Hooke in the rule "ut tensio sic vis" which means that stresses and strains follow each other proportionally. The development of elasticity generalized this to a tensorial relationship between stress and strain whose possible forms can be simply grasped by considering the elastic energy [11, 13, 15].

We shall call in the remainder $\underline{\gamma}$ and $\underline{\sigma}$ the strain tensor and the stress tensor, $(i, j)$ the indexes of the coordinates tangent to the sheet, and $k$ the index of the normal coordinate to the sheet. The volumic density of elastic energy $\varepsilon$ will then satisfy $\partial \varepsilon / \partial \gamma_{ij} = \sigma_{ij}$.

Reducing attention to sheets here enables one to decompose stresses into their average along the sheet depth, $\bar{\sigma}_{ij}$, and the complementary part $\sigma'_{ij}$: $\sigma_{ij} = \bar{\sigma}_{ij} + \sigma'_{ij}$.

**Fig. 7.4** Strain in a sheet made of the uniform stretching part $\bar{\gamma}$ and the flexural part $\gamma'$ equal to the difference of strains with respect to the mid-height surface (*dotted line*)
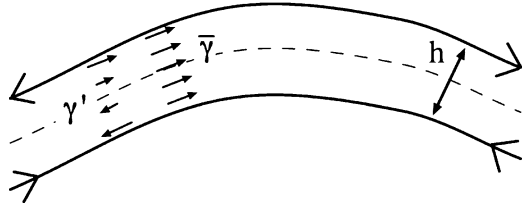


The former stress corresponds to viewing the sheet as a superposition of identical 2D surfaces and the latter stress expresses the actual differences undergone by these surfaces depending on their position on the sheet depth: $\sigma'_{ij}$ depends on $x_k$.

As 2D surfaces have zero thicknesses, their stresses only refer to stretching. However, following sheet curvature, the different surfaces which compose a sheet actually experience different strains since outer or inner surfaces stand at slightly different distances from the curvature centers. They thus involve some differences that are related to curvature. Within the thin sheet approximation, one can assume a linear variation of the complementary stresses $\sigma'_{ij}$ with the normal component $x_k$: $\sigma'_{ij} \propto x_k$, the origin $x_k = 0$ being placed at the middle of the sheet thickness. Then the stresses $\sigma_{ij}$ involve a mean part $\bar{\sigma}_{ij}$ independent of $x_k$ and a complementary part $\sigma'_{ij}$ linearly varying with $x_k$: $\sigma'_{ij} = x_k \tilde{\sigma}'_{ij}$. The same is true for the corresponding strains $\underline{\gamma} = \underline{\bar{\gamma}} + \underline{\gamma}'$ with $\underline{\bar{\gamma}}$ and $\underline{\gamma}'$, respectively, independent of and proportional to $x_k$: $\gamma'_{ij} = x_k \tilde{\gamma}_{ij}$ (Fig. 7.4).

By definition, the surfacic energy density $e$ satisfies $\delta e = \int \sigma_{ij} \delta \gamma_{ij} dx_k$, the integral being taken between $\pm h/2$, $h$ designing the sheet thickness. Integration thus yields $\delta e = \delta e_s + \delta e_b$ with $\delta e_s = h \bar{\sigma}_{ij} \delta \bar{\gamma}_{ij}$ and $\delta e_b = \frac{h^3}{12} \tilde{\sigma}'_{ij} \delta \tilde{\gamma}_{ij}$. Here $e_s$ denotes a stretching energy density and $e_b$ a bending energy density. Interestingly, $e_s$ is proportional to $h$ but $e_b$ is proportional to $h^3$.

On this basis, the objective remains to clarify the link between stress and strain. For this, a convenient way consists in using the elastic energy, thanks to its scalar nature. This, together with an emphasis on the role of the Gaussian curvature, will yield the expression of the link between sheet form and elastic stresses in equilibrium states in the form of the Föppl–von Kármán equations.

## 7.3.1 Sheet Elastic Energy

Following the linear relationship between stress and strain, the volumic elastic energy density $\varepsilon$ is quadratically related to the strain tensor $\underline{\gamma}$. However, the energy density being scalar, it must be related to those parts of the strain tensor that are scalar and, because of global rotational invariance, isotropic. These constraints select two candidates only, the trace of the tensor square $\text{Tr}(\underline{\gamma}^2)$ and the square of the tensor trace $[\text{Tr}(\underline{\gamma})]^2$, yielding a simple relationship with coefficients $\lambda$ and $\mu$

called Lamé coefficients: $\varepsilon = \frac{1}{2}\lambda\,[\mathrm{Tr}(\underline{\gamma})]^2 + \mu\,\mathrm{Tr}(\underline{\gamma}^2)$. Two coefficients only are thus required to characterize an elastic medium. Formally, they are actually the analogous of the two viscosities required to characterize a viscous fluid.

Given the expression of the elastic energy density of a volumic material, one now wishes to apply it to the specific case of a thin sheet whose strain tensor $\underline{\gamma}$ can be decomposed into a thickness-uniform strain tensor $\bar{\underline{\gamma}}$ and a linearly thickness-dependent strain tensor $\underline{\gamma}'$: $\underline{\gamma}' = -x_k\underline{C}$. Here, the tensor $\underline{C}$ corresponds to the curvature tensor defined by $C_{i,j} = \mathbf{n}\partial^2\mathbf{r}/(\partial x_i\partial x_j)$. The dependence on $x_k$ then states that the sheet surface that is the farthest from the center of curvature is stretched whereas that which is the nearest from this center is compressed, as compared to the mid-thickness surface $x_k = 0$ (Fig. 7.4).

Integration of the volumic energy density over the sheet thickness yields:

* No cross contribution between $\bar{\underline{\gamma}}$ and $\underline{\gamma}'$, i.e., between stretching and bending, for parity reason in $x_k$
* A surfacic stretching energy $e_{\mathrm{s}} = \frac{h}{2}[\lambda\,[\mathrm{Tr}(\bar{\underline{\gamma}})]^2 + \mu\,\mathrm{Tr}(\bar{\underline{\gamma}}^2)]$
* A surfacic bending energy $e_{\mathrm{b}} = \frac{h^3}{24}[\lambda\,[\mathrm{Tr}(\underline{C})]^2 + \mu\,\mathrm{Tr}(\underline{C}^2)]$

Here, both the strain tensors $\bar{\underline{\gamma}}$ and $\underline{C}$ only depend on the in-plane components $x_i, x_j$ and are thus 2D. Interestingly, the trace of their square then satisfies $\mathrm{Tr}(T^2) = \mathrm{Tr}(T)^2 - 2\mathrm{Det}(T)$, as may be directly checked from the algebra of 2*2 matrices. As their trace and their determinant easily express as the sum and the product of their eigenvalues, it appears convenient to rewrite the surfacic energies in term of them:

* $e_{\mathrm{s}} = \frac{h}{2}\frac{E}{(1-v^2)}\{[\mathrm{Tr}(\bar{\underline{\gamma}})]^2 - 2(1-v)\mathrm{Det}(\bar{\underline{\gamma}})\}$.
* $e_{\mathrm{b}} = \frac{h^3}{24}\frac{E}{(1-v^2)}\{[\mathrm{Tr}(\underline{C})]^2 - 2(1-v)\mathrm{Det}(\underline{C})\}$ where $v = \lambda/2(\lambda+\mu)$ is the Poisson ratio and $E = \mu(3\lambda+2\mu)/(\lambda+\mu)$ the Young modulus.

Regarding the bending energy density, we note that $\mathrm{Tr}(\underline{C}) = c_1 + c_2$ corresponds to the sum of the principal curvature, $c_1$, $c_2$, and thus to twice the mean curvature $C = (c_1 + c_2)/2$. On the other hand, $\mathrm{Det}(\underline{C})$ stands as the product of the principal curvatures, i.e., the Gaussian curvature $G$. The bending energy density thus also expresses as $e_{\mathrm{b}} = B[2C^2 - (1-v)G]$ where $B = \frac{h^3}{12}\frac{E}{(1-v^2)}$ is the bending modulus.

### 7.3.2 Gaussian Curvature and Theorema Egregium

Among the deformations that can be undergone by a sheet, it will appear relevant to determine the characteristics of those that induce no stretch, i.e., the isometric deformations. In 2D, they correspond to global translations and rotations. In 3D, they may also include curvature modes, i.e., bending, under conditions to clarify.

Quite generally, for a 3D volume, the evolution of its metrics may be deduced from that of elementary distances $ds$ between nearby points $M$ and $M + \mathbf{dM}$. Calling
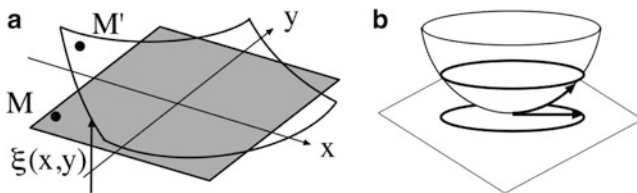
**Fig. 7.5** (**a**) Gauss' Theorema Egregium. One considers a mapping $M \rightarrow M'$ from the plane $(x, y)$ to the surface $z = \xi(x, y)$. For an isometric mapping to exist, the Gaussian curvature of the surface must be equal to that of the plane, i.e., zero. (**b**) An axisymmetric mapping from the plane to the paraboloïd that would preserve the perimeter of a circle would inevitably stretch its radius, as expected from the difference of Gaussian curvature between the plane $(G = 0)$ and the paraboloïd $(G > 0)$

$\mathbf{u}(M)$ the displacement undergone by a point $M$, one gets $dM_i = dx_i$ in the rest state and $dM_i = dx_i + \partial u_i / \partial x_j dx_j$ in the stretched state, the space directions being indexed $(i, j, k)$. The distance squared between nearby points $ds^2 = \mathbf{dM}^2$ then reads $ds^2 = dM_i dM_i = g_{ij} dx_i dx_j$ and thus $g_{ij} = \delta_{ij}$ in the rest state and $g_{ij} = \delta_{ij} + 2\gamma_{ij}$ in the stretched state, the strain tensor $\underline{\gamma}$ being $\gamma_{ij} = 1/2(\partial u_i / \partial x_j + \partial u_j / \partial x_i) + 1/2(\partial u_k / \partial x_i)(\partial u_k / \partial x_j)$.

Let us first start by determining to what conditions on a surface of cartesian equation $\xi(x, y)$ can an elementary isometric mapping exist between the plane $z = 0$ and this surface (Fig. 7.5a). Any mapping between the plane $(x, y, 0)$ and the surface $(x', y', z' = \xi(x', y'))$ involves the displacement $(u, v, w) = [x' - x, y' - y, \xi(x', y')]$. Isometry imposes that the elementary length elements on the plane and on the mapped surface are the same: $ds^2 = ds'^2$ with $ds^2 = dx^2 + dy^2$ and $ds'^2 = dx'^2 + dy'^2 + dz'^2$. To express this constraint, let us notice that the latter expression writes $ds'^2 = dx^2(1+a) + dy^2(1+b) + 2c\, dxdy$ with $a = 2\partial_x u + (\partial_x \xi)^2$, $b = 2\partial_y v + (\partial_y \xi)^2$, $c = \partial_y u + \partial_x v + \partial_x \xi \partial_y \xi$. Isometry therefore imposes $a = b = c = 0$. This requirement may be transposed to a constraint on the sole surface $\xi(x, y)$ by noticing that the mapping $(u, v)$ disappears from the combination $c - (a + b)/2 = 0$ which reads: $\partial_x^2 \xi \partial_y^2 \xi - (\partial_x \partial_y \xi)^2 = 0$.

A simple geometrical interpretation of this condition may be obtained by considering, up to a global rotation, the cartesian axes as the principal curvature axes of the surface, so that $\xi = \frac{1}{2} c_1 x^2 + \frac{1}{2} c_2 y^2 +$ h.o.t., $c_1$, $c_2$ denoting the principal curvatures and h.o.t. "higher order terms". The above criterion then reduces to $c_1 c_2 = 0$. More generally, the left-hand side of this criterion appears proportional to the determinant of the curvature tensor, $\text{Det}(\underline{C})$, and thus of the Gaussian curvature $G = c_1 c_2$. Accordingly, the condition for an isometric mapping to exist from a plane to a surface is that its Gaussian curvature is zero: $G = 0$.

One may straightforwardly generalize this constraint to isometric mappings from one surface, not necessarily a plane, to another, respectively, indexed 1 and 2. For this, one simply has to state that the evolution of their metrics from their tangent plane is the same: $ds'_1{}^2 = ds'_2{}^2$, this common length evolution being possibly not

zero. The above algebra then shows that this turns back to the equality of their $a$, $b$, and $c$ terms and thus of their combination $c - (a+b)/2$ or, equivalently, of their Gaussian curvature.

One obtains this way the Gauss' Theorema Egregium which states that isometric mappings must conserve Gaussian curvatures. In turn, any change of Gaussian curvature will indicate a change of metrics, i.e., a stretch. This way be illustrated on the elementary surface $\xi = \frac{1}{2}c_1 x^2 + \frac{1}{2}c_2 y^2 + \text{h.o.t.}$ considered above by noticing that, for equal curvature $c_1 = c_2 = c$, and thus for nonzero $G = c^2$, the axisymmetric mapping from the plane to this surface which would preserve the perimeter of the circle of radius $r$ would inevitably stretch its radius (Fig. 7.5b).

### 7.3.3 Sheet Equilibrium and Föppl–von Kármán's Equation

Consider a weakly distorted sheet from its planar state $(x, y, 0)$, its distortion being described by the equation $z = \xi(x, y)$, and focus attention to an elementary part of it with normals **n** at the boundaries. Its equilibrium condition requires mechanical equilibrium on the in-plane directions and on the normal direction:

∗ In-plane directions: no gain of momentum is allowed from the flux of stretching stresses $\bar{\sigma} = \underline{\bar{\sigma}} \mathbf{n}$ at its boundaries: $\text{div}(\underline{\bar{\sigma}}) = 0$. This requirement for a 2D in-plane tensor $\underline{\bar{\sigma}}$ imposes that it derives from a scalar potential, the Airy potential $\chi$, such that $\bar{\sigma}_{ij} = (-1)^{i+j} \partial^2 \chi / \partial x_i \partial x_j$.
∗ Normal direction: for a bent sheet, the normal component of the net contribution of stretching stresses applied at its boundaries must equilibrate that provided by bending. The former is proportional to $h$ and may be expressed with the Airy potential. This yields the first Föppl–von Kármán equation:

$$B \triangle^2 \xi - h[\xi, \chi] = 0 \tag{7.1}$$

where the first term denotes bending contribution, the second the stretching contribution, and the brackets, the Poisson brackets $[U, V] = \partial_{ii}^2 U \partial_{jj}^2 V + \partial_{ii}^2 V \partial_{jj}^2 U - 2\partial_{ij}^2 U \partial_{ij}^2 V$.

The second Föppl–von Kármán equation corresponds to a compatibility condition for stresses to derive from strains induced by an actual displacement. This condition corresponds to the above relationship $c - (a+b)/2 = 0$ for isometric mappings and, more generally, $c - (a+b)/2 = G$ for mappings inducing a Gaussian curvature. Relating strains to stresses and then to the Airy potential yields:

$$\triangle^2 \chi + E[\xi, \xi] = 0 \tag{7.2}$$

where $[\xi, \xi] = G$ for weakly distorted surfaces.

These two equations describe the relationships between stresses ($\chi$) and geometry ($\xi$) for weakly distorted sheets at equilibrium.

## 7.4  Experiment

The experiment aims at compressing a thin sheet while keeping one of its principal curvature fixed at a nonzero value. For this, one seeks to compress a sheet in between parallel cylinders so that their curvature radius $R$ fixes one sheet's principal curvature [14]. To this end, the sheet is clamped by two of its sides on a cylinder along a direction normal to the cylinder generatrix. This will then force the fold axes to adopt the cylinder curvature (Fig. 7.6).

### 7.4.1  Setup

The compression setup is shown in Fig. 7.7. It consists in a fixed upper plate and a moving lower plate in between which the sheet to compress is placed. The lower plate is pushed up by a piston placed at the middle of the system but is blocked by three stepper motors before touching the upper plate. These motors thus enable to monitor the gap $Y$ between the compressing plates to an accuracy of a tenth of microns.

The upper plate is taken transparent so as to allow visualization from above. For the present experiment, the plates, usually flat, have been replaced by cylinders made of plexiglass for the upper plate and of polycarbonate for the lower plate. Thin rulers enable the sheet to be clamped on the curved sides of the lower cylindrical plate. Visualization of the sheet form has been achieved by illuminating it from the sides with two different colors, red and blue. This way, the image recorded by a camera fixed on top of the setup could make the difference between right and left sides of the sheet folds, thus improving the contrast and the understanding of the sheet form.

The sheet is made of polycarbonate and has the following dimensions: length $l = 155$ mm, width $L = 190$ mm, and thickness $h$ ranging from 0.05 mm to 0.5 mm. It is clamped along its length onto the bottom cylinder. As the distance between the clamping arches, $X = 180$ mm, is smaller than the sheet width $L$, the sheet is thus already buckled before compression (Fig. 7.8). Finally, the cylinder curvature radius, $R = 50$ cm, is taken large compared to the few millimeters gap $Y$ and thus to the fold sizes, so as to make the configuration locally close to a compression between parallel plates.
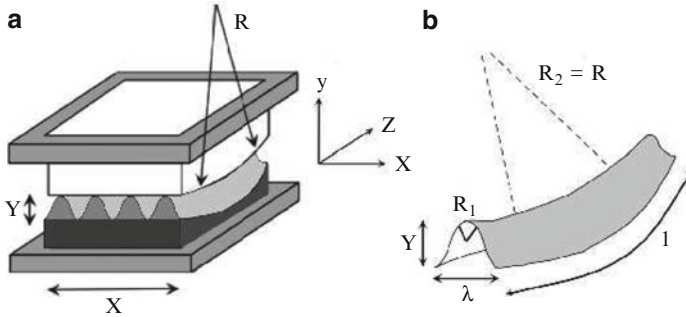
**Fig. 7.6** A compressing device (**a**) involves cylindrical plates distant from a controlled gap $Y$ with, in between, a sheet clamped on their curved sides. (**b**) By iterative buckling, gap reduction yields the generation of folds of ever smaller size $\lambda$, whose axis is bent by the cylinders. This results in two principal curvatures $c_1 \sim \lambda^{-1}$, $c_2 \sim R^{-1}$ and thus in Gaussian curvature and in-plane stretching

**Fig. 7.7** Snapshot of the setup used to perform and study sheet compression. A bottom plate is pushed up by a piston and blocked by stepper motors, leaving a gap $Y$ to a fixed top plate. Sheets are clamped on one of the plates and compressed as the gap $Y$ decreases. Visualization is achieved from above thanks to a transparent top plate
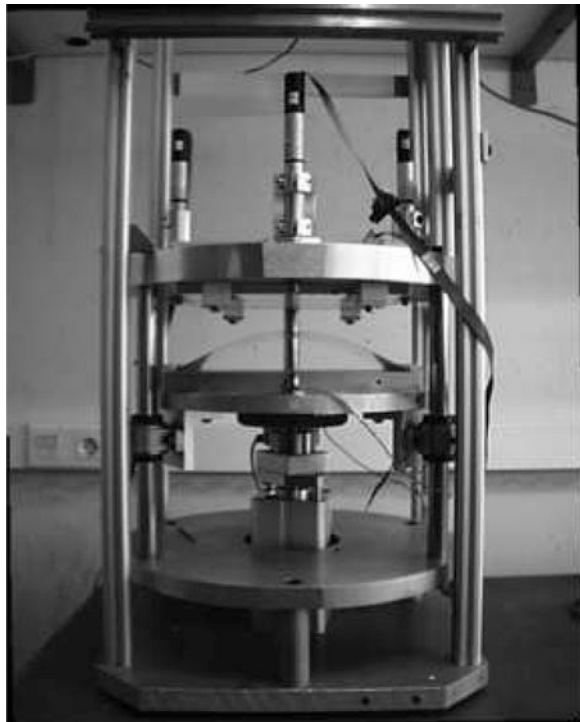


## 7.4.2  Compression Route

The cylinder curvature radius being large, the compression route shares some analogy with the Elastica route [18–20]. In particular, a buckling cascade is observed with the fold number ever increasing as compression proceeds (Fig. 7.9). Following
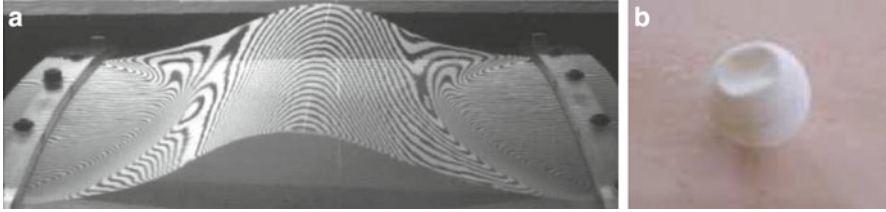
**Fig. 7.8** (**a**) Clamped sheet prior compression showing two ridges at the contact lines between the sheet and the cylinder. (**b**) Buckled ping-pong ball showing ridges where large curvature and stretch are focused

the invariance of the compressing cylindrical plates on both the clamping direction (same curvature along it) and its normal (straight cylinder axis), the sheet folds, either smooth or singular, show the same shapes. In particular, their common width $\lambda$ follows the gap $Y$ in the sense that the ratio $\lambda/Y$ varies in a short range that depends on the excess length $L/X$ and which corresponds in practice here to the range $[20/3, 9]$. The largest bound corresponds to buckling folds and the lowest bound to just buckled folds. Accordingly, the number $n = X/\lambda$ of folds varies as $nY = XY/\lambda$, with $nY$ bounded in the range $[X/9, 3X/20]$, i.e., $[20, 27]$ mm here.

Without compression, the clamped sheet shows two domains in contact with the cylinder with a fold in between (Fig. 7.8a). The frontier between them corresponds to an elastic defect, the so-called "ridge", on which curvature is focused. It is analogous to that observed on a buckled ping-pong ball (Fig. 7.8b) [11, 21] and on which stretching yields plastic deformation. However, it is actually weaker in the sense that no plastic transition is triggered here.

As compression proceeds together with the resulting successive bucklings, the sheet shows first ridges at its contact with cylinders (Fig. 7.9a, b), as on the uncompressed state of Fig. 7.8. However, on further compression, another kind of defect appears, the d-cone (Fig. 7.9c, d, e).

This kind of defect corresponds to those found when distorting a planar sheet by pressing it with a sharp tip [10, 12]. All the stress is then focused on this tip, leaving the remaining of the sheet unstretched. One may observe that the sheet is not axisymmetric with respect to the tip axis but shows a folded circumference that makes the difference with a cone. This traces back to the fact that the cone is not a developable surface, i.e., that it cannot be continuously mapped onto a plane without cutting it somewhere. This indicates that some Gaussian curvature is in order, not on the cone sides since they are curved on a single direction but at the cone tip where all the stretch is thus concentrated [9, 10]. However, in comparison, the planar sheet making a d-cone is actually developable since it was initially planar. The difference between both is the folded part of the distorted planar sheet which, if removed, could yield an actual cone.
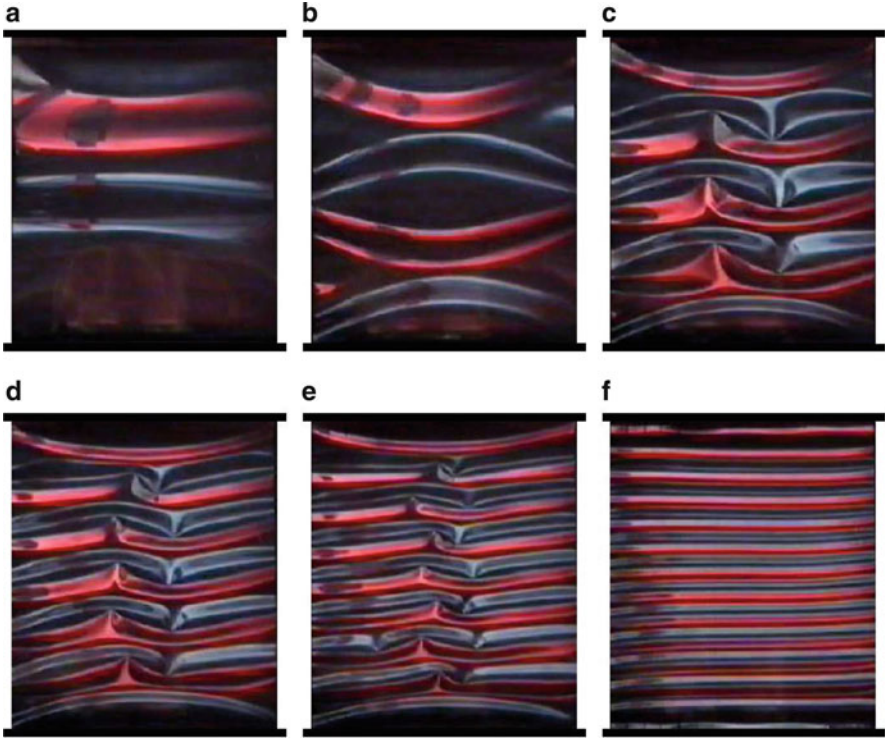
**Fig. 7.9** Experimental pictures taken from above; $h = 180$ microns. Colors refer to left (*red, bright*) or right (*blue, bright*) fold sides. Clamped sides are shown by black ticks. Compression increases from (**a**) to (**f**). (**a**) Single fold with ridge. (**b**) Two folds with ridges. (**c**) (**d**) (**e**) Four, six, and eight folds with ridges and d-cones. (**f**) Regular state of twelve folds involving *no* singularity

These d-cones thus involve a large curvature at the tip of the sharp tongue they display (Fig. 7.9c, d, e) with, therefore, a large stretch there. In contrast, they enable the stretch to be removed from the remaining of the sheet, as on the canonical example of a sheet pressed with a tip [10].

The number of d-cones increases with the fold number, each fold displaying its d-cone (Fig. 7.9a, b). Accordingly, focusing stress on the tip of elastic defects seems to be the nominal mean for self-organizing the sheet so as to adapt compression. Viewed this way, there should be no reason to self-organize differently when compressing further. However, somewhat surprisingly, beyond a fold number $n = 11$, all d-cones *spontaneously disappear* from the bulk leaving a smooth, regular, state, free of elastic defect (Fig. 7.9f) [14]. Then, further increasing simply yields further buckling with no longer any defect occurrence.

It should be noticed that the regular state made of parallel defect-free folds nevertheless involves stretch and nonzero Gaussian curvature $G$ since the fold axes are bent by the cylinders. However, the difference with the defect state is that this

**Fig. 7.10** Critical number of folds $n_c$ at the uncrumpling transition for different sheet thicknesses $h$. Continuous line corresponds to $2\pi\gamma_c n_c = (hR/2X^2)^{-1/2}$ with $\gamma_c = 0.55$ as best fitting coefficient. Inset: same data in log-log scales
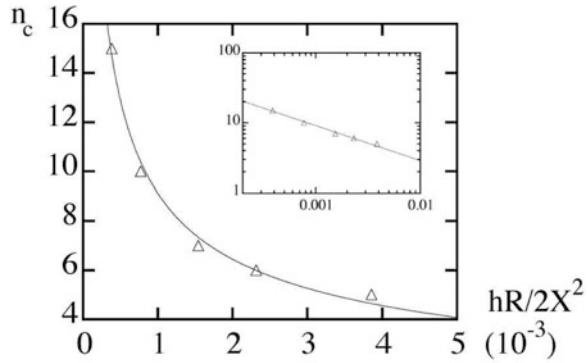


stretch is distributed on the whole sheet instead of being concentrated in localized areas. The morphological transition on defect appearance/disappearance therefore corresponds to a transition from a condensed stretch to a distributed stretch or, equivalently, to a stress-defocusing process. The remaining of this study is devoted to understand it.

## 7.4.3 Defocusing Scaling

At a defect core, the sheet can no longer be viewed as a 2D surface (or a collection of superimposed 2D surfaces) and must be considered as three-dimensional. This means that the sheet thickness should parametrize the defect occurrence or disappearance and thus the stress-defocusing phenomenon. Similarly, the fact that both stretch and curvature are involved in the sheet organization converges to the same conclusion since they scale differently with the thickness $h$. These remarks thus invite us to vary the sheet thickness and address the resulting modification of stress defocusing.

Varying $h$ by a factor of 10, from 0.05 to 0.5 mm at otherwise same length and width, we observed similar routes exhibiting the same qualitative events and only displaying quantitative variations. In particular, the fold number $n_c$ at which stress defocusing occurs has been found to vary with $h$ as a power law: $n_c \propto h^{-1/2}$ (Fig. 7.10). The fact that $n_c$ scales with $h$ gives confidence for using this relationship to infer relevant information on stress defocusing. In particular, as the relevant characteristic scales playing on $n_c$ are the cylinder radius $R$, the distances $X$ between arches, the sheet width $L$, and the sheet thickness $h$, one may expect from dimensionality a scaling relationship of the kind $n_c \propto (R/h)^\alpha (X/h)^\beta (L/h)^\gamma$. The objective of the modeling will thus be to determine these exponents and recover the observed fact that their sum is $1/2$.

## 7.5  Energy Criterion for Stress Focusing and Scalings

In the introduction, we have argued that energy could help in clarifying the origin of stress defocusing and more generally the self-organization of elastic sheets within the prescribed boundaries. The argument consists in identifying the observed state with the less energetic state, leaving aside the issue regarding the path required to change state and, therefore, possible metastability. Here, we would like to make this argument quantitative so as to recover the location of stress defocusing on the compression route and especially the power law variation $n_c(h)$.

For this, we thus address the energy criterion for defocusing and express it by using scaling arguments [14].

### 7.5.1  Energy Criterion for Stress Focusing or Defocusing

Our goal is to compare the sheet elastic energy $E$ in a stress-focused state and in a stress-defocused state. This energy expresses as the integral over the sheet surface of its energy density $e$: $E = \int_{\text{sheet}} e \, ds$. Here $e$ can be decomposed in a bending contribution $e_\text{b}$, a stretching contribution $e_\text{s}$, and a defect contribution $e_\text{d}$, the two formers being referring to the sheet except the defect core and the latter to these defect cores. To facilitate the comparison, we shall denote the stress-focused state with the superscript "f" and the stress-defocused state with the superscript "d."

As the less energetic state is favored, the criterion reads:

- Stress focusing: $E^f \ll E^d$.
  There is an energetic gain to focus stress in defects.
- Stress defocusing: $E^d \ll E^f$.
  There is an energetic gain to defocus stress on the whole sheet.
- Stress focusing/defocusing transition: $E^d \sim E^f$.
  Both energies being similar, there is no clear advantage in one or the other state.

In the defocused states, the defect energy density vanishes by definition: $e_\text{d}^d = 0$. On the other hand, the absence of multiple characteristic scales on these states allows the scaling of the evolutions with compression to be determined from the Föppl–von Kármán equations for both the bending and the stretching energy densities, $e_\text{s}^d$, $e_\text{b}^d$. Accordingly, in defocused states, one should be able to follow the evolution of the sheet energy $E^d$ with the fold number $n$, as compression proceeds.

By comparison, in the focused states, a similar determination is delicate owing to a more complex geometry of the sheet states and to the difficulty in expressing the energy density $e_\text{d}^f$ on a defect without solving for its inner structure. However, denoting $\rho$ the size of the defect core, its energy is about $B(\rho/h)^{1/3}$ [13] and, as $\rho \sim h$, of the order of $B$, i.e., of the sheet bending energy. Accordingly, we may omit this defect energy in the evaluation of $E^f$ without noticeable implication on the determination of the transition. In particular, as we expect a variation of

several orders of magnitude of the balance between the energies of the focused and defocused states, order one differences between the different terms are irrelevant. On the other hand, the stretching energy density $e_s^f$ in the focused states is for sure largely reduced compared to its defocused value, so that it no longer stands as the dominant energy density. We shall then assume that it is of the same order of the bending energy density $e_b^f$ which, on the other hand, should remain comparable to its defocused value: $e_s^f \sim e_b^f \sim e_b^d$. Accordingly, we shall thus consider the bending energy as representative of the order of magnitude of the energy density $e^f$ of the focused state: $e^f \sim e_b^f \sim e_b^d$.

The transition criterion $E^f \sim E^d$ then reads $e_b^d \sim e_s^d + e_b^d$ or, equivalently, $e_s^d \sim e_b^d$. Interestingly, it is thus expressed on the defocused state only, which we know and can evaluate. Its physical meaning is that defects actually relax the stretching energy density $E_s$ on the whole sheet, leaving the bending energy $E_b$ plus the defect energy $E_d$, which are of the same order. This is obviously energetically favorable when the stretching energy is dominant on regular states, i.e., when $e_s^d >> e_b^d$, in which case defects should occur. On the opposite, for $e_s^d \sim e_b^d$, regular states should be maintained. The criterion for a transition between focused and defocused states is thus $e_s^d / e_b^d \sim O(1)$.

### 7.5.2   Scalings

The compression route shows two imbricated phenomena: buckling and defect occurrence/disappearance. The former yet occurs on compression between parallel plates, i.e., for $R = \infty$, and the latter is specific of a finite $R$. Let us address them successively, first within the Elastica and then within the Föppl–von Kármán equations.

Elastica involves no Gaussian curvature and no stretch. The only source of stresses is thus bending via flexural terms. As a consequence, there is no longer a scaling competition between stretching ($\propto h$) and bending ($\propto h^3$), so that the sheet thickness $h$ only serves to gauge stresses and forces without implication on the sheet state. In particular, the sheet behavior satisfies scale invariance with respect to $h$.

This scale invariance enables us to relate states by zooming them in and out. Consider a $n$-fold solution obtained after several bucklings (e.g., a fourfold solution in Fig. 7.3-left). Each fold is physically equivalent to the onefold solution found prior to buckling. Both are connected by a zoom such that the fold of the fourfold solution whose width is $X/n$ is mapped onto the onefold whose width is $X$, i.e., by a zoom factor of $X/(X/n) = n$. Accordingly, the folds corresponding to characteristic lengths $(Y/n, X/n)$ and $(Y, X)$ are geometrically similar (and also dynamically similar as shown in [18–20]). This, in particular, states that the fold width $\lambda$ and the fold height $Y$ scale like $n^{-1}$.

Let us now consider curved plates, i.e., a large but finite $R$, and determine how scalings operate in a situation where stretching and bending compete on a defocused state. In particular, our objective is to express the evolution of the stretching and bending energy densities as compression proceeds.

Regarding the bending energy density, $e_b = B[2C^2 - (1-\nu)G]$, one may notice that, when integrated over the whole sheet, the contribution of the Gaussian curvature is constrained by the Gauss–Bonnet theorem [22] which states that the integral of $G$ over a compact surface is related to a topological invariant, the Euler characteristics of the surface, and to the boundary integral of the geodesic curvature at the surface boundary. On the other hand, the small curvature of the cylinders negligibly changes the sheet form at its boundaries so that the boundary integral and finally the surfacic integral of $G$ hold a value close to the one they have for a compression between planes. However, as the Gaussian curvature vanishes in this case, its net integral contribution would be zero for such a compression between plane and, by extension, for the present compression between cylinders. For this reason, we shall skip the contribution of $G$ to the bending energy density $e_b$ hereafter and reduce it to $e_b = 2BC^2 \sim Eh^3C^2$.

Regarding the stretching energy density $e_s$, its definition $\delta e_s = h\bar{\sigma}_{ij}\delta\bar{\gamma}_{ij}$ with $\bar{\gamma} \sim \bar{\sigma}/E$ shows that its scalings follow those of the combination $h\bar{\sigma}^2/E$ where $\bar{\sigma}_{ij} = (-1)^{i+j}\partial^2\chi/\partial x_i\partial x_j$, the Airy potential satisfying $\triangle^2\chi + EG = 0$. To evaluate them, let us model the regular folds by the surface $\xi(x,z) = \xi_0(x) + z^2/2R$, where $\xi_0 \approx (Y/2)\sin(2\pi x/\lambda)$ is a $\lambda$-periodic function and where the dependence on $z$ conveys the fold curvature imposed by the cylinders. Spatial derivatives then extract the length scale $\Lambda = \lambda/(2\pi)$ so that $\Lambda^{-4}\chi \sim EG$, $\sigma \sim \Lambda^{-2}\chi$ and, finally, $e_s \sim Eh\Lambda^4G^2$.

Altogether, this yields the transition criterion $e_s/e_b = O(1)$ with $e_s/e_b \sim \gamma^4 = O(1)$ and $\gamma = \Lambda(G/hC)^{1/2}$. We stress that it applies on any compression route of thin sheets.

On the original compression route between cylinders studied here, one has $c_1 \sim Y/\Lambda^2$, $c_2 \sim 1/R$ with $c_1 \gg c_2$ and thus $C \sim c_1/2$ and $G/C \sim 2c_2$. This, with $\lambda \sim n^{-1}$, yields $\gamma = (\lambda/2\pi)(2/hR)^{1/2} \sim n^{-1}$ and thus an order parameter for the transition varying sensitively with the fold number $n$ as $e_s/e_b \sim \gamma^4 \sim n^{-4}$. This sensitivity to the fold number then relativizes the role of prefactors in the above scaling relationships and therefore supports the analysis.

Calling $\gamma_c$ the value of $\gamma$ at the transition, the above expression of $\gamma$ yields the critical fold number at the transition: $n_c = (hR/2X^2)^{-1/2}/2\pi\gamma_c$. One thus recovers the experimental scaling evidenced in Fig. 7.10 with a computed value $\gamma_c \sim 0.76$ of order one, as expected for the transition.

## 7.6 Phase Diagram and Nature of Singularities

Following the above criterion, we are now able to determine the conditions required for focusing or defocusing stress in a sheet and synthesize them in a phase diagram [14]. This will be especially useful to interpret the three canonical compression

routes that are compared in Sect. 7.2. However, before turning attention to this quantitative view, it is instructive to realize that the surprising phenomenon of defocusing is a simple logical consequence of scale invariance.

### 7.6.1  Scale-Invariance and Defocusing

Three characteristic lengths are in order on a sheet state: (1) a fold morphological scale, the fold width $\lambda$, for instance, (2) the cylinder curvature radius $R$, and (3) the sheet thickness $h$. These are in particular the three variables which enter the transition criterion.

The fact that, in contrast to Elastica, $h$ is a relevant scale here forbids the different states of a given compressed sheet to be geometrically similar, since any homothety would ask to change the sheet thickness. This, however, does not forbid to use scale invariance to compare, at fixed thickness $h$, the evolutions undergone when varying $\lambda$ with respect to $R$ or vice versa.

In particular, let us consider the change of fold width $\lambda$: $(\lambda, R, h) \to (\alpha\lambda, R, h)$. Owing to the absence of intrinsic scale in elasticity, i.e., to its scale-invariant nature, similar states may be obtained by changing the scale of *all* lengths by the *same* factor. Accordingly, the latter state $(\alpha\lambda, R, h)$ is equivalent to $(\lambda, R/\alpha, h/\alpha)$.

Moreover, in our configuration where a principal curvature $c_1$ is much larger than the other $c_2$, the Föppl–von Kármán Eqs. (7.1) and (7.2) involve a scale invariance focused on the couple of scales $(R, h)$. This may be evidenced by noticing that, as $c_1 >> c_2$, the laplacian operator reduces to $\triangle\xi \approx \partial^2\xi/\partial x^2$, so that $\triangle^2\xi \approx \partial^4\xi/\partial x^4$. Note that, in these relationships, the equality is even actually achieved within the modeling of the sheet's surface $\xi(x, z) = \xi_0(x) + z^2/2R$. As, from relation (7.2), the Airy potential follows the modulations of the sheet's surface, the same conclusion may be drawn for it: $\triangle^2\chi \approx \partial^4\chi/\partial x^4$. In this instance, it then appears that, as $B \sim Eh^3$, the Föppl–von Kármán Eqs. (7.1) and (7.2), respectively, agree with the following scaling relationships $\chi x^2 \sim h^2 z^2$ and $\chi z^2 \sim x^2\xi^2$ where variables are used here to denote their scale (e.g. $\partial^4\chi/\partial x^4 \sim \chi/x^4$ or $[\xi, \chi] \sim \xi\,\chi\,x^{-2}\,z^{-2}$). These relationships are equivalent to $\chi \sim x^2 \sim hz$, since by definition $\xi \sim z$. A class of scale change which satisfies these scaling constraints is the following: $(x, z, \xi, \chi, h) \to (x, \beta^{-1}z, \beta^{-1}\xi, \chi, \beta h)$. It means that an increased thickness $h$, $h \to \beta h$, goes together with an anisotropic zoom $(x, z) \to (x, \beta^{-1}z)$. As the curvature $R^{-1}$ corresponds here to $\partial^2\xi/\partial z^2 \sim z^{-1}$, one gets $R \sim z$ and thus the following change for $R$, $R \to \beta^{-1}R$. This therefore corresponds to an actual invariance for both $x$ (and thus $\lambda$) and the combination $Rh$: $x \to x$, $Rh \to (\beta^{-1}R)(\beta h) = Rh$. An echo of this property is found in the fact that, besides $\lambda$, the variables $R$ and $h$ enter the transition parameter $\gamma$ through this combination $Rh$.

According to this additional symmetry, the state $(\lambda, R/\alpha, h/\alpha)$ is also physically equivalent to $(\lambda, R/\alpha^2, h)$. So are therefore the states $(\alpha\lambda, R, h)$ and $(\lambda, R/\alpha^2, h)$ which interestingly display the same thickness $h$. Accordingly a decrease of $\lambda/R$ at *fixed* $h$ can be equally obtained in two physically equivalent ways:

(1) By increasing $R$ at *fixed* $\lambda$ and $h$: $(\lambda, R, h) \to (\lambda, R/\alpha^2, h)$, $\alpha < 1$
(2) By decreasing $\lambda$ at *fixed* $R$ and $h$: $(\lambda, R, h) \to (\alpha\lambda, R, h)$, $\alpha < 1$

   With this in mind, we now compare two compression routes, the first route referring to the sole variation of $R$ at fixed $\lambda$ and $h$, and the second route referring to the sole variation of $\lambda$ at fixed $R$ and $h$ (Fig. 7.11). One recognizes in the first route the bending of a fold axis and in the second route, the compression between cylinders worked out here. Both however refer to a variation of the ratio $\lambda/R$ at fixed $h$ and should thus tell the same story.

- First route: fold bending
  Bending the axis of a fold turns out increasing its principal curvature $c_2 = 1/R$ from zero at a fixed $\lambda$, i.e., at a fixed principal curvature $c_1$. As one may easily figure out, this yields the generation of defects, actually d-cones, beyond some critical value of $c_2$.
  This route, which corresponds to decreasing the ratio $c_1/c_2 = \lambda/R$, thus shows us that stress focusing should be encountered this way.
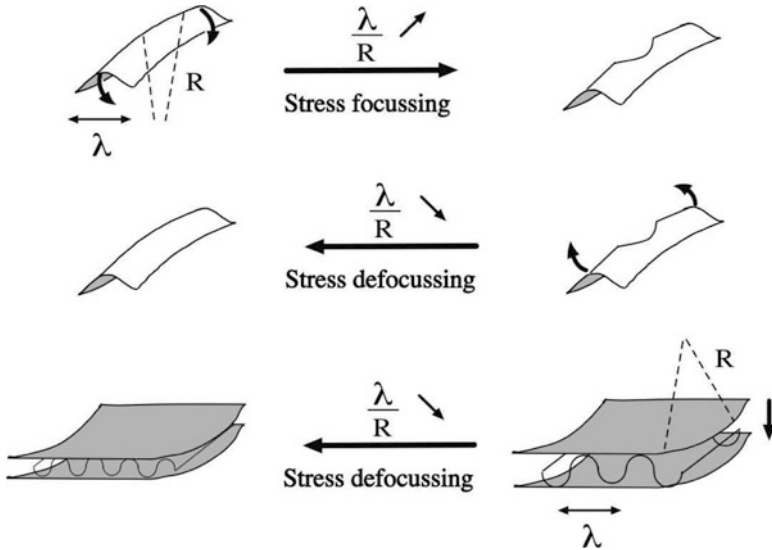- Second route: compression between cylinders
  Compressing a sheet between cylinders turns out decreasing the fold width $\lambda$ by iterated buckling at fixed $R$, i.e., at fixed $c_2$. This corresponds to increasing the principal curvature $c_1 \sim \lambda^{-1}$ at fixed $c_2$ and, therefore, to increasing the ratio $c_1/c_2 \sim \lambda/R$. From this point of view, this route corresponds to an opposite direction of compression as compared to the first route. Both routes being similar as viewed with respect to the ratio $c_1/c_2$ at fixed $h$, this means that one should encounter defocusing on the second route as surely as one encounters stress focusing on the first route.

   This simple reasoning naturally explains why compression between cylinders should yield defocusing despite the general increase of stress undergone by the sheet (Fig. 7.11). It emphasizes that the thing which matters regarding the occurrence or not of defects is not the global amount of stress but its balance between stretch and bending on regular states. In particular, reducing the fold width by iterated buckling renders the curvature radius of their axis apparently larger, as compared to their width. This corresponds to decreasing the effective bending of their axis, i.e., to rendering them more straight, until this bending becomes small enough for defocusing to occur.

### 7.6.2 Scalings and Phase Diagram for Singularities

The transition criterion $\gamma = \Lambda(G/hC)^{1/2} = \gamma_c = O(1)$ derived in Sects. 7.5.1 and 7.5.2 applies to any states of thin sheets. It thus enables us to determine the domains where focused or defocused stress are in order.
   Before applying this to work out a phase diagram for stress focusing, we would like to turn from the geometrical expression of the criterion in terms of mean

**Fig. 7.11** Equivalence between fold de-bending and compression between cylinders. Fold bending increases $\lambda/R$ and yields stress focusing. Fold de-bending therefore reduces $\lambda/R$ by variation of $R$ and yields stress defocusing. Similarly, compression between cylinders together with iterated buckling makes $\lambda/R$ also decrease but by variation of $\lambda$. As for fold de-bending, this must therefore also yield defocusing

curvature $C$ and Gaussian curvature $G$ to an expression in terms of typical strains relative to curvature $\gamma_C$ or stretch $\gamma_G$. The decomposition of strains in Sect. 7.3.1 shows that $\gamma_C$ may be taken as $hC$.

The determination of stretching stresses from the Airy potential in Sect. 7.3.3 together with scaling arguments similar to those applied in Sect. 7.5.2 shows that $\gamma_G \sim \sigma/E \sim \Lambda^{-2}\chi/E$ with $\chi \sim \Lambda^4 EG$, so that $\gamma_G \sim \Lambda^2 G$. Altogether this yields the transition criterion to read $\gamma = (\gamma_G/\gamma_C)^{1/2} = \gamma_c = O(1)$.

In the variable space $(\gamma_C, \gamma_G)$ and in logarithmic coordinates, the transition criterion thus corresponds to a straight line whose slope is $1/2$ and which is located according to the experimental value 0.55 of $\gamma_c$. Above this line, one finds focussed singular states and below it defocused regular states (Fig. 7.12).

Let us now place the compression routes in this diagram:

- Elastica
  The Elastica corresponds to $\gamma_G = 0$ and thus to a horizontal line with an ordinate repelled up to $-\infty$. Whereas we cannot reproduce it on the diagram, we may realize that it stands within the regular, defocused, domain.
- Crumpled paper
  Because of isotropy, all the length scales and especially the fold widths and the two principal curvature radii take similar values. Accordingly $\Lambda^2 \sim 1/G$ so that $\gamma_G \sim O(1)$. This compression route thus corresponds to a horizontal line located
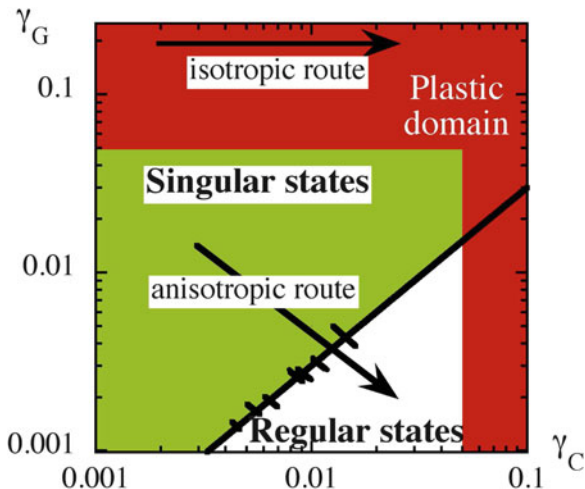
**Fig. 7.12** Transition diagram in the variable space $(\gamma_C, \gamma_G)$, where $\gamma_G = hC$ and $\gamma_G = \Lambda^2 G$ are the typical strains due to curvature and to in-plane stretching. The isotropic route always lies in the plastic domain. In contrast, anisotropic crumpling yields elastic regularization and stress defocusing before experiencing plastic deformation. The thick line corresponds to the uncrumpling transition for $\gamma_c = 0.55$ and black ticks to the observed uncrumpling transition for $h$ varying from 50 to 500 microns, including error bars. Note that the diagram would be similar in variables $(G/C^2, hC)$

at values of ordinates about unity. It thus stands within the singular, focused, domain till the first stage of compression (Fig. 7.12). Accordingly, defects should occur at the very beginning of the compression of a paper sheet in hands, as may be directly confirmed in practice. However, they should also encounter the transition to defocusing at large compression, a fact which is not corroborated in practice, for reasons explained below.

- Compression between cylinders
  Here $c_1 \sim Y/\Lambda^2$, $c_2 \sim 1/R$ with $c_2 \ll c_1$. This yields $\gamma_C \sim hY/\Lambda^2$, $\gamma_G \sim Y/R$. In addition, following buckling, $\Lambda$ and $Y$ decrease similarly so that $\Lambda \sim Y$. This finally yields $\gamma_G \sim (h/R)\gamma_C^{-1}$, i.e., a line with slope $-1$ and located according to the value of $h/R$. As displayed in Fig. 7.12, it crosses the transition diagram from the singular, focused, domain to the regular, defocused, domain, as compression proceeds.

These compression routes, which are reported in the phase diagram of Fig. 7.12, thus well reproduce the experimental evidence, except for the crumpled paper which is found to neither defocus stress nor remove defect at large compression. This discrepancy will be explained below by plasticity.

This phase diagram provides a new vision of singularity occurrence in elasticity. Instead of being viewed as objects forced by external means, by frustration, or by boundary conditions, they simply appear here as a possible expression of a sheet

state, besides an alternative one corresponding to a stress smoothly distributed on a geometrically regular state. In particular, we note that the disappearance of singularities under compression evidenced here differs from that observed when pressing a fold with a sharp tip [23] in the sense that singularities disappear here in the bulk whereas they are expelled to the sheet boundary in the latter case. This difference emphasizes the fact that stress focusing or defocusing stands here as a bulk matter, actually the spontaneous selection of a preferred phase under constraint. This therefore makes this elastic issue close to a thermodynamic issue, the different routes being simply different kinds of path followed in phase space.

Attached to this thermodynamic view is the requirement that forming singularities do not change physics irreversibly, since making a closed path in phase space should yield back to the starting phase. This is actually satisfied in this experiment of compression between cylinders since decompressing the sheet yields back to the starting planar sheet without evidence of the history. Such a reversibility is however not involved in paper crumpling since permanent scars are generated. This calls for completing the phase diagram by taking into account plasticity. Of course, as this complement will not concern the whole phase diagram but only a part of it, it does not break the thermodynamic interpretation but simply complete it with an additional phenomenon.

### 7.6.3   Plasticity

Plastic deformations occur at too large strains. Then the sheet escapes the linear elasticity domain within which removing the stress makes the system return to its initial strain. This therefore results in irreversible deformations that are located where the strains were too large, i.e., here, at the defect cores.

A criterion for a transition to plasticity is the occurrence of strains larger than a threshold value, typically a few percent, actually 5 % here [24]. This yields us to complete the phase diagram by restricting the linear elasticity domain to a square domain located at low strains. Interestingly, this discriminates the different routes addressed here since the isotropic compression route corresponding to crumpled paper entirely lays in the plastic domain whereas the anisotropic route provided by compression between cylinders stands in the elastic one. Their different behaviors regarding stress defocusing are then naturally explained: whereas both should display defocusing at large compression, the isotropic route will not since the plastic transition preempts the defocusing transition; however, the anisotropic route will, provided the regular states are not too much compressed before experiencing defocusing.

As for other thermodynamic transitions, this complete phase diagram opens strategic choices to achieve sheet compressions that might avoid plasticity or not, visit the singularity domain or not, keep within the regular domain or not, etc. These different strategies might correspond to interesting practical issues in mechanics, electronics, or in compaction.

## 7.7   Conclusion

Crushing a paper in a ball yields the generation of scars which denote a transition from a regular geometry to a singular geometry. Meanwhile the stress distribution changes from regularly distributed to condensed on singularities, a phenomenon called stress focusing. The relevant stress part in this focusing refers to the stretch induced by a nonzero Gaussian curvature $G = c_1 c_2$ where $c_i$ denotes the principal curvatures at a point. Usually, two compression routes are investigated, the Elastica routes where $G = 0$ and the isotropic compression routes where $c_1 \sim c_2$. The former then yields no singularity whereas the latter corresponds to crumpled paper. However, as two curvatures are in order in $G$, intermediate routes may exist to explore the full bi-dimensionality of the issue. The objective of this study has been to manage the compression configuration so as to address one of them here. It consists in compressing a sheet between cylinders so as to increase a principal curvature $c_1$ only, while keeping the other one $c_2$ constant.

Interestingly, compressing a sheet this way generated singularities which surprisingly spontaneously all disappeared at large compression. This unintuitive stress defocusing by compression is at variance with the view that could be inherited from crumpled paper. We explained it qualitatively by showing from scale invariance of the Föppl–von Kármán equations that the reduction by buckling of the width of the folds that are bent by the cylinders is physically equivalent to decreasing the bending of the axes of folds of fixed width. As the latter route removes the singularities that could have appeared at large axis bending, it corresponds to a stress defocusing. The same phenomenon is thus in order by compressing folds between cylinders and may be qualitatively understood by the fact that cylinders seem all the more flat as the folds are small.

This interpretation has been made quantitative from scaling arguments which have been applied on a criterion for defocusing. This criterion states that, as defects relax stretch and decrease the stretching energy, it is advantageous to focus stress only if the stretching energy is large compared to the bending energy. This was synthesized on a phase diagram in which a transition line separates the domain where stress is focused from the one where it is defocused. The bidimensionality of this diagram echoes the existence of two relevant modes for stresses (stretch and bending) or for strains (Gaussian curvature and mean curvature). In particular, the different routes addressed here highlight the existence of two principal curvatures whose features vary according to the compression protocol.

To explain the formation of irreversible scars, the phase diagram has been completed with plastic domains. This shows that the plastic transition may preempt or not the defocusing transition depending on the compression route. In particular, it actually preempts it on the isotropic configuration of crumpled paper but not on the anisotropic compression routes investigated here since defocusing occurs on them prior to plasticity. Accordingly, crumpled paper appears as a misleading example of elasticity since the structures it shows, the singularities, should have disappeared if the plastic transition had not occurred. In this sense, it is a combined example of elasticity plus plasticity. On the opposite, the defocusing phenomenon exhibited here by compression between cylinders fully refers to linear elasticity from which it naturally derives thanks to scale invariance.

These results provide a renewed view of singularities according to which they are understood as the expression of an elastic singular phase in competition with a regular defocused phase. Within this thermodynamic interpretation, the bidimensionality of the phase diagram allows the elaboration of strategies regarding crushing. In particular, using cylinders instead of plates to compress sheets enabled us to remove singularities before encountering plastic transition. This could find interesting practical applications for instance for compressing more material sheets without altering them.

# References

1. V. Pereira, A. Castro Neto, H. Liang, L. Mahadevan, Phys. Rev. Lett. **105**, 156603 (2010)
2. J. Genzer, J. Groenewold, Soft. Matter **2**, 310 (2006)
3. U. Seifert, Adv. Phys. **46**, 13 (1997)
4. M. Alava, K. Niskanen, Rep. Prog. Phys. **69**, 699 (2006)
5. M. Golombek, F.S. Anderson, M.T. Zuber, J. Geophys. Res. **106**, 811 (2001)
6. A. Lobkovsky, S. Gentges, H. Li, D. Morse, T. Witten, Science **270**, 1482 (1995)
7. A. Lobkovsky, Phys. Rev. E **53**, 3750 (1996)
8. A. Lobkovsky, T. Witten, Phys. Rev. E **55**, 1577 (1997)
9. M. Ben Amar, Y. Pomeau, Proc. R. Soc. Lond **A 453**, 729 (1997)
10. E. Cerda, L. Mahadevan, Phys. Rev. Lett. **80**, 2358 (1998)
11. B. Audoly, Y. Pomeau, *Elasticity and Geometry: From Hair Curls to the Non-Linear Response of Shells* (Oxford University Press, Oxford, 2010)
12. S. Chaïeb, F. Melo, J.C. Géminard, Phys. Rev. Lett. **80**, 2354 (1998)
13. T. Witten, Rev. Mod. Phys. **79**, 643 (2007)
14. B. Roman, A. Pocheau, Phys. Rev. Lett. **108**, 074301 (2012)
15. L. Landau, E. Lifshitz, *Theory of Elasticity* (Elsevier, Cambridge, England, 1986)
16. L. Euler, *Methodus Inveniendi Lineas Curvas Maximi Minimivi Propreitate Gaudentes. Additamentum I: De curvis elasticas* (Lausanne & Geneva, 1744)
17. W.A. Oldfather, C.A. Ellis, D. Brown, Isis **20**, 72 (1930)
18. B. Roman, A. Pocheau, Europhys. Lett. **46**, 602 (1999)
19. B. Roman, A. Pocheau, J. Mech. Phys. Sol. **50**, 2379 (2002)

20. A. Pocheau, B. Roman, Physica D **192**, 161 (2004)
21. A. Pogorelov, *Bendings of Surfaces and Stability of Shells* (American Mathematical Society, Providence, 1988)
22. D.J. Struik, *Lectures on Classical Differential Geometry* (Addison-Wesley, Reading, 1961)
23. A. Boudaoud, P. Patricio, Y. Couder, M. Ben Amar, Nature **407**, 718 (2000)
24. B. Du, O.C. Tsui, Q. Zhang, T. He, Langmuir **17**, 3286 (2001)